JMEPEG (2010) 19:1065–1070
DOI: 10.1007/s11665-009-9584-6

1059-9495/$19.00

Creep Life Prediction of Thermally Exposed Rene 80 Superalloy

M. Aghaie-Khafri and S. Farahany

(Submitted September 10, 2008; in revised form July 23, 2009)

The effects of long time thermal exposure on the microstructure and mechanical properties of Rene 80 superalloy were investigated by means of scanning electron microscopy and accelerated creep tests at 190 MPa and 980 °C. Results obtained showed that the rupture lives of pre-exposed samples decreased by increasing the exposure time or exposure temperature. In addition, as a new finding the concept of contour maps of the constant life and minimum creep rate were introduced. These maps were used to estimate the effect of exposure time and exposure temperature on the creep rupture life and minimum creep rate of thermally exposed samples.

Keywords creep, heat treating, mechanical testing, non-ferrous metals and alloys, scanning electron microscopy, superalloys

1. Introduction

Rene 80 is an investment casting superalloy which is frequently used for high-temperature applications, especially for blades and vanes in gas turbines. During the service exposure at high temperatures; however, critical components of gas turbine engines are being degraded. The degradation phenomenon consists of either purely physical alternations or metallurgical damages which reduced the capability of hot sections to resist service stresses. This drastically decreases the service life of the rotating sections which are located in the vicinity of the hot gas inlet (Ref 1-3).

At the high-operating temperatures within a gas turbine, creep damage is a major life limiting factor. Thereby, a number of life prediction techniques based on the correlation between rupture life and creep characteristics have been improved. The Sherby-Dorn life prediction method is based on a temperature adjusted time parameter. This parameter is derived by considering the expression for the secondary creep strain rate at constant stress (Ref 4). The Larson-Miller parameter is similar to the Sherby-Dorn parameter, but different assumptions were made in its derivation (Ref 5). The Larson-Miller method is a reliable technique for life prediction as long as the alloy microstructure is stable during prolonged exposure at high temperature (Ref 6, 7). Monkman and Grant (Ref 8) proposed an extrapolation technique for high temperature-high stress creep-rupture data based on the relationship between steady-state creep rate and rupture life.

The aim of this study was to evaluate the influence of long time thermal exposure on the microstructure and high-temperature creep deformation of Rene 80 nickel base superalloy.

2. Experimental Procedures

2.1 Materials and Processing

The chemical composition of the cast Ni-base polycrystalline superalloy Rene 80 is given in Table 1. The raw material was produced by vacuum melting process. Prism-shaped specimens with a size of $10 \times 10 \times 5$ mm^3 were prepared from the as-received material. These specimens subsequently were subjected to standard heat treatment (SHT). The SHT for Rene 80 included the following steps.

Heat to 1204 °C for 2 h followed by furnace cool to 1093 °C within 10 min.
Hold at 1093 °C for 4 h, furnace cool to 649 °C within 60 min, and hold at 649 °C for 10 min.
Raise temperature to 1054 °C and hold for 4 h, cool to 649 °C within the range of 15-60 min, and hold for 10 min.
Raise temperature to 843 °C and hold for 16 h, then air cool to room temperature.
To examine the effect of thermal exposure, SHT samples were exposed at high temperatures in an atmospheric furnace. The exposure time was 100, 500, and 1000 h and the exposure temperatures were 800, 850, and 900 °C.

2.2 Microstructure Evaluation

The study of microstructure characteristics of the virgin and heat-treated material after thermal exposure was conducted by means of light microscopy and scanning electron microscopy. Samples for optical microscopy were mounted, mechanically grinded, and polished according to the standard procedure and subsequently etched in Marble etchant, which has a chemical

M. Aghaie-Khafri and **S. Farahany**, Faculty of Mechanical Engineering, K.N. Toosi University of Technology, P.O. Box 19395-1999, Tehran, Iran. Contact e-mail: maghaei@kntu.ac.ir.

Table 1 Chemical composition of Rene 80 in wt.%

	Cr	C	Mo	W	Ti	Nb	Co	Al	B	Fe	Zr	Ni
Rene 80	13.4	0.16	4.11	3.92	4.77	0.03	9.45	2.12	0.02	0.10	0.04	Balance

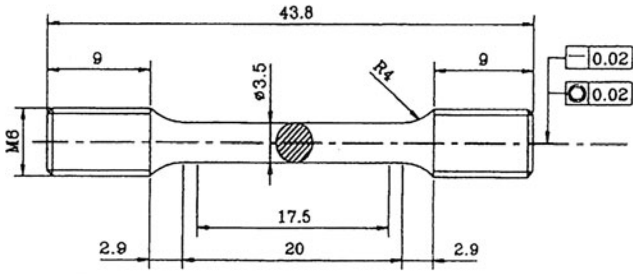

Fig. 1 Creep test specimen where dimension is in millimeter

composition as following 10 g $CuSO_4$, 50 mL HCl, and 50 mL H_2O. For scanning electron microscopy examination, samples were electro polished with a solution of 10% HCl + methanol at 20 V for 20 s. Samples were subsequently electro etched with 170 mL phosphoric acid + 10 mL sulfuric acid and 16 g chromium trioxide at 5 V for 3-5 s.

2.3 Accelerated Creep Test

The creep tests were carried out using virgin and exposed specimens. The cylindrical specimens were machined according to the drawing shown in Fig. 1. The gauge length was 17.5 mm, and the diameter of the specimens was 3.5 mm. The creep load to produce average stress of 190 MPa was applied and testing temperature was 980 °C. The creep tests were performed until the rupture of the specimens. The temperature was monitored by three type K thermocouples and maintained within about ±2 °C. The average stress rupture properties obtained on three test specimens for each experimental condition were reported.

3. Results and Discussion

3.1 Microstructure

Optical micrograph of the as-cast Rene 80 is shown in Fig. 2. Microstructure of the as-cast sample consists of two phase γ-γ' microstructure with the dendrite segregation pattern. It is worth noting that heavy elements such as W and Mo with high melting points tend to segregate at the core of dendrites, causing a bright region. However, the interdenrite darker region of as-cast microstructure was enriched in Al and Ti (Ref 9, 10).

The microstructure of heat-treated sample (Fig 3) mainly consists of FCC γ Ni-base matrix, carbides and dispersion of the intermetallic γ' precipitate phase. It is clear the SHT developed a duplex size distribution of the γ' precipitates generally identified as primary and secondary gamma prime. The γ' Ni_3Al (Ti, Nb) intermetallic precipitate phase has the ordered structure of the Cu_3Au-type. This phase is responsible for the extraordinary high-temperature properties of the alloy (Ref 11). In the present investigation, the average diameter of primary and secondary γ' of SHT samples was 0.285 and the total γ' volume fraction was determined to be 45-50%.

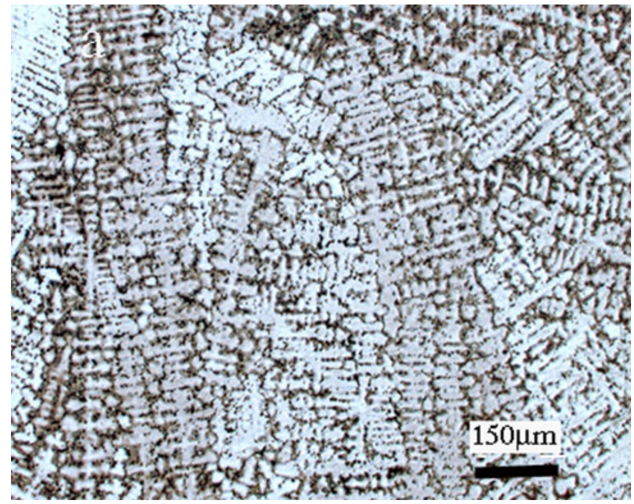

Fig. 2 Microstructure of the as cast Rene 80 sample

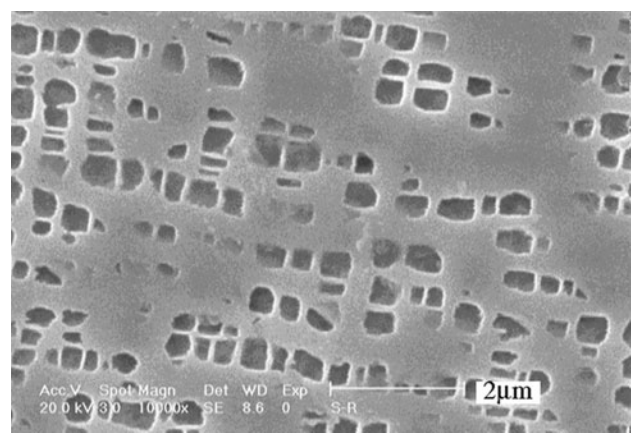

Fig. 3 Microstructure of the Rene 80 sample after standard heat treatment

Service exposed blades show a series of microstructural changes which are a function of time, temperature, and stress (Ref 12, 13). In particular, the γ' precipitates tend to agglomerate. However, carbide reactions cause the formation of undesirable continuous carbide films along grain boundaries as shown in Fig. 4. Chemical analysis of carbides identifies that the carbides formed within grains are mainly MC-type carbides, in which M is substituted for Ti, W, and Ta. The carbides observed at grain boundaries are M23C6-type carbides, in which M is substituted for Cr and Mo.

Microstructure of exposed sample at 900 °C for 1000 h is shown in Fig. 5. It is clear that the shape of γ' precipitates in the matrix has been changed from cuboidal to round one. In addition, the size and the fraction of γ' were changed. Considering the calculation of the precipitate diameter,

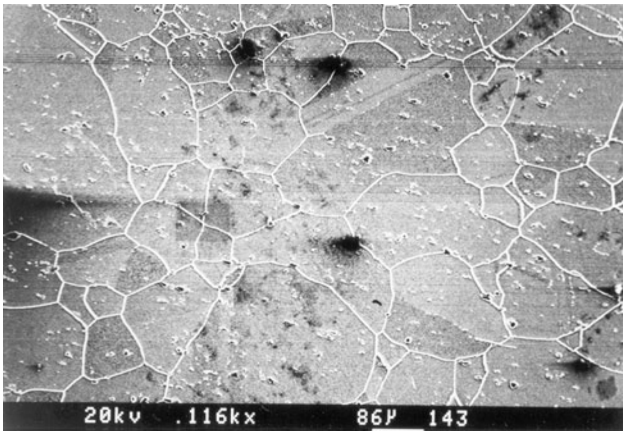

Fig. 4 Formation of continuous network of carbides along the grain boundaries in service exposed Rene 80 blade

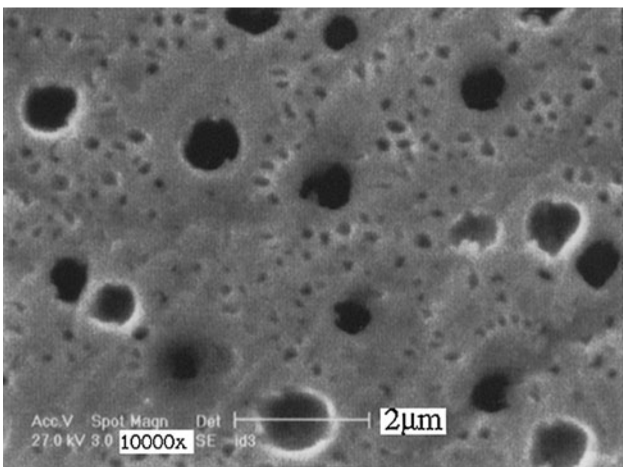

Fig. 5 Microstructure of the SHT sample after exposure at 900 °C for 1000 h

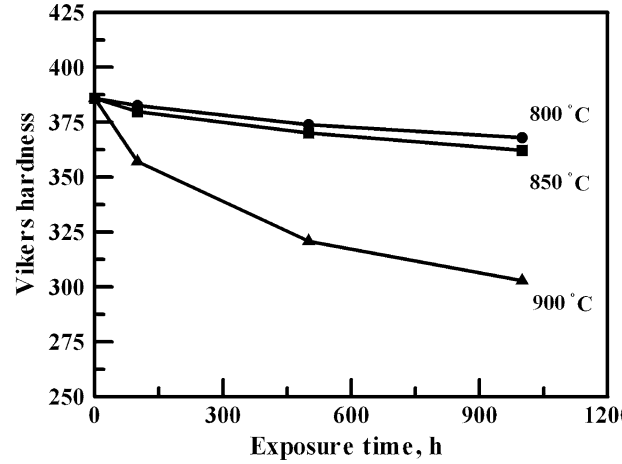

Fig. 6 Variation of hardness of Rene 80 samples with exposure time at different exposure temperatures

Table 2 Mean γ′ diameter (μm) for exposed samples at different exposure temperature (*T*) and exposure time (*t*)

	T, °C		
***t*, h**	**800**	**850**	**900**
100	0.291	0.301	0.319
500	0.307	0.336	0.398
1000	0.316	0.396	0.479

Table 3 Results of creep test at 980 °C and 190 MPa for virgin and pre-exposed samples

Exposure temperature, °C	Exposure time, h	Rupture time, h	Reduction of area, %	Minimum creep rate, 1/h
…	…	46.5	19.1	1.815e−4
800	100	46.2	20.2	1.990e−4
800	500	44.8	17.3	2.302e−4
800	1000	43.9	15.7	2.342e−4
850	100	42.5	17.1	2.312e−4
850	500	36.1	12.1	2.989e−4
850	1000	31.6	10.6	3.144e−4
900	100	40.2	14.4	3.185e−4
900	500	32.2	19.4	3.809e−4
900	1000	27.6	14.2	4.530e−4

diameters of spherical particles were directly measured and for cuboids particles the equivalent circle diameter was determined on the basis of the area measurement. Average size of γ′ precipitates for exposed specimens are presented in Table 2. The observed phenomenon of coarsening has a detrimental effect on the mechanical properties, particularly on the creep properties at the service temperature.

3.2 Hardness and Creep Degradation

Hardness of virgin material was decreased from 359 to 302 HV following thermal exposure at 900 °C for 1000 h. The effect of thermal exposure time on the hardness of Rene 80 samples at different temperatures is shown in Fig. 6. It is clear that the hardness decreased with increasing the time of thermal exposure. This effect is more severe at higher temperatures, especially at 900 °C.

Steady-state creep rates, time to rupture and reduction of area at failure for virgin, and exposed samples tested in air at 190 MPa and 980 °C are reported in Table 3. It is worth noting rupture life of virgin material decreased by a factor of 1.7 and steady-state creep rate decreased by a factor of 2.5 following thermal exposure at 900 °C for 1000 h. Considering microstructural degradation, diameter of γ′ precipitate increased by a factor of 1.7. Consequently, microstructural evolution during thermal exposure has a main effect on mechanical properties of exposed specimen.

The variations of creep rupture life and minimum creep rate versus exposure time for Rene 80 at different exposure temperatures are shown in Fig. 7 and 8, respectively. It is evident that rupture lives of the samples decreased linearly with increasing exposure time. It is worth noting the slope of the lines are steeper at higher temperatures, causing shorter creep rupture lives at 850 and 900 °C.

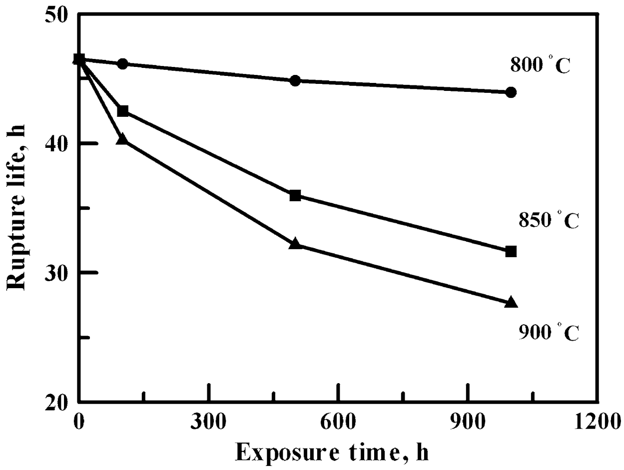

Fig. 7 Variation of stress rupture life of Rene 80 samples with exposure time at different exposure temperatures

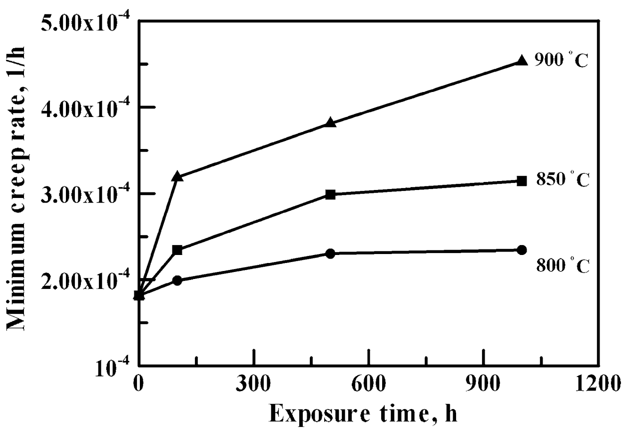

Fig. 8 Variation of minimum creep rate of Rene 80 samples with exposure time at different exposure temperatures

3.3 Isolife Contour Map

The rupture time, t_r, of the pre-exposed creep specimens can be expressed as

$$t_r = f(t, T), \quad \text{(Eq 1)}$$

where t and T are exposure time and temperature, respectively. Considering the creep results for virgin and exposed specimens (Table 3), a cubic spline fit for the test data is used to generate a greater number of data points. Subsequently, the computed data are graphically represented by a contour map of constant life as shown in Fig. 9 where the lives of the thermally exposed samples were designated by the contour numbers. The constructed isolife diagram can be used for prediction of the rupture lives of service exposed components at a known working stress and temperature (i.e., 190 MPa and 980 °C in Fig. 9). Furthermore, different parametric techniques can be used for remaining life assessment of the components.

A comprehensive interpretation of the isolife map requires a thorough understanding of the creep mechanisms at different regions. It is generally accepted that creep mechanisms at different conditions are governed by the minimum creep rate.

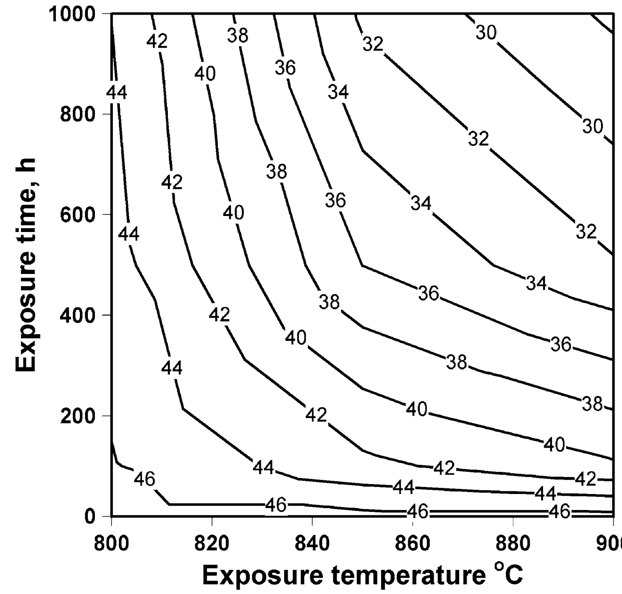

Fig. 9 Isolife contour map of Rene 80 where contour numbers represent stress rupture life (h) of specimens at different conditions

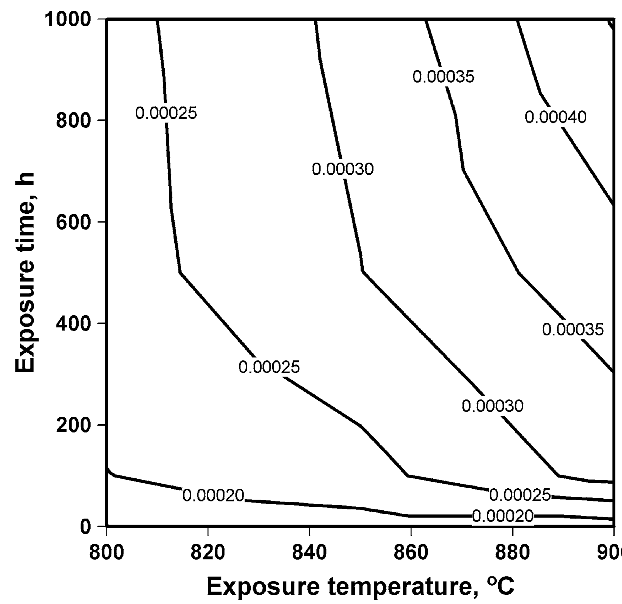

Fig. 10 Contour map of the minimum creep rate for Rene 80 where contour numbers represent minimum creep rates (1/h) at different conditions

Figure 10 shows the contour map of the minimum creep rate at different exposure time and temperatures. Different regions in the map can be attributed to a specific microstructure degradation which affects the deformation mechanism.

3.4 Effect of γ' Coarsening on Rupture Life

It is well known that coarsening of the γ' precipitates during exposure at high temperature is a key factor responsible for creep degradation of Ni-base superalloys (Ref 14). In this case, according to Lifshitz, Slyozov, and Wagner (LSW) theory (Ref 15, 16), coarsening process is driven by the reduction in

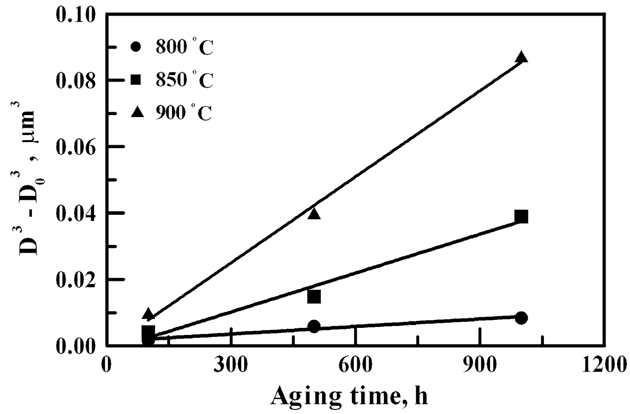

Fig. 11 The variations of $D^3 - D_0^3$ vs. time for γ' precipitates

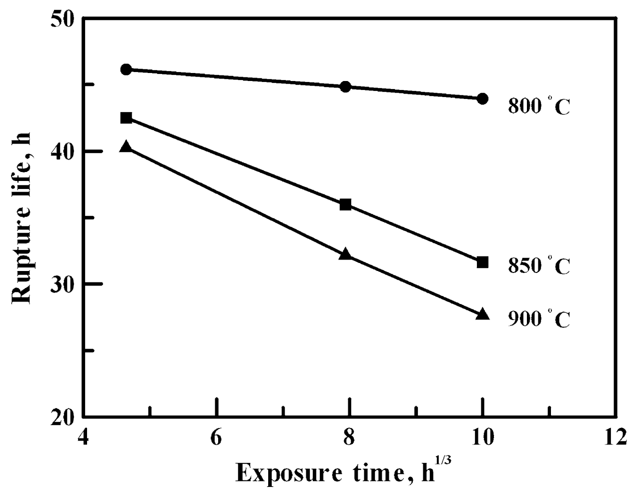

Fig. 12 A plot of variation of rupture life vs. exposure time

total interfacial energy. Consequently, the growth kinetics would follow an equation expressed by:

$$D^3 - D_0^3 = Kt, \qquad \text{(Eq 2)}$$

where t is the exposure time, D_0 and D are the average size of γ' precipitates before aging ($t = 0$) and at the time t, respectively. K is the rate constant and is a function of temperature. The variations of $D^3 - D_0^3$ versus time for γ' precipitates are shown in Fig. 11. It is clear the coarsening kinetics for the γ' precipitates follows closely a linear line which is in good agreement with the LSW theory.

Considering Eq. 2, rupture life, t_r, should be a function of exposure time, $t^{1/3}$, and can be expressed as

$$t_r = At^{1/3}, \qquad \text{(Eq 3)}$$

where A is rate constant and is a function of temperature. Figure 12 shows the variation of rupture time versus $t^{1/3}$ at different exposure temperatures. It is clear that the experimental results follow a straight line as predicted by Eq 3.

It is generally accepted that there is a correlation between mechanical properties degradation of the thermally exposed samples and changes in size and density of γ' precipitates (Ref 3). The variation of rupture life with diameter of γ' is

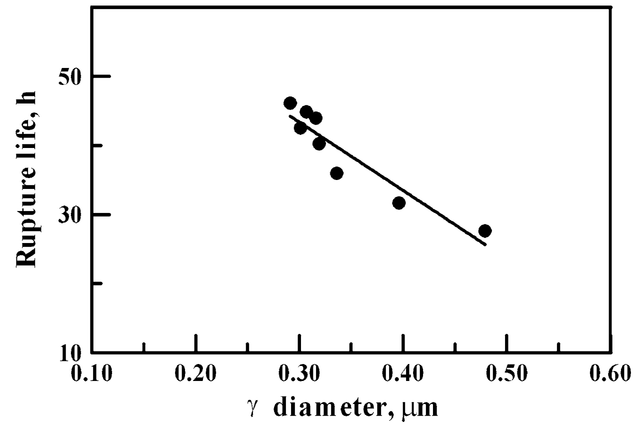

Fig. 13 The variation of rupture life with diameter of γ'

shown in Fig. 13. It is clear that rupture life of the specimens steeply decrease with increasing γ' diameter. Therefore, the variation of γ' size has a major effect on the degradation of thermally exposed samples.

4. Conclusions

The following conclusions from high-temperature accelerated creep testing and microstructure analysis of pre-exposed Rene 80 samples can be drawn.

- The hardness and creep lifetime of the Rene 80 superalloy decreased after long time thermal exposure. The coarsening of γ' precipitates is the main factor responsible for the mechanical properties degradation of the alloy.
- Contour maps of the constant life and minimum creep rate were introduced. These maps clearly show the effect of exposure time and temperature on the creep rupture lives of the specimens.
- Concerning the LSW theory and the correlation between the coarsening and creep degradation, the rupture life of pre-exposed samples, t_r, predicted as $t_r = At^{1/3}$, where t is exposure time and A is a rate constant.

References

1. T.M. Maccagno, A.K. Koul, J.P. Immarigeon, L. Cutler, R. Allem, and G. Lesperance, Microstructure, Creep Properties, and Rejuvenation of Service-exposed Alloy 713C Turbine Blades, *Metall. Trans. A*, 1990, **21**, p 3115–3125
2. J.A. Brown, R. Freer, and A.T. Rowley, Reconditioning of Gas Turbine Components by Heat Treatment, *ASME J. Eng. Gas Turb. Power*, 2001, **123**, p 57–61
3. R. Viswanathan, *Damage Mechanisms and Life Assessment of High-Temperature Components*, ASM International, Ohio, 1989
4. R. Orr, O.D. Sherby, and J.E. Dorn, Correlation of Rupture Data for Metals at Elevated Temperatures, *Trans. ASME*, 1954, **46**, p 113–118
5. F.R. Larson and J. Miller, A Time-Temperature Relationship for Rupture and Creep Stress, *Trans. ASME*, 1952, **74**, p 756–775
6. A.K. Koul and R. Castilo, Assessment of Service Induced Microstructural Damage and Its Rejuvenation in Turbine Blades, *Metall. Trans. A*, 1988, **19**, p 2049–2066

7. G. Marahleh, A.R.I. Kheder, and H.F. Hamad, Creep-Life Prediction of Service-Exposed Turbine Blades, *Mater. Sci. Eng. A*, 2006, **433**, p 305–309
8. F.C. Monkman and N.J. Grant, *Proc. ASTM*, 1956, **56**, p 593–620
9. G.E. Fuchs, Solution Heat Treatment Response of a Third Generation Single Crystal Ni-Base Superalloy, *Mater. Sci. Eng. A*, 2003, **300**, p 52–60
10. J. Safary and S. Nategh, On the Heat Treatment of Rene-80 Nickel-Base Superalloy, *J. Mater. Process. Technol.*, 2006, **176**, p 240–250
11. C.T. Sims, N.S. Stoloff, and W.C. Hagel, *Superalloys II*, Wiley, New York, 1972, p 98–131
12. J. Zrnik, P. Strunz, V. Vrchovinsky, O. Muransky, Z. Novyc, and A. Wiedenmann, Degradation of Creep Properties in a Long-Term Thermally Exposed Nickel Base Superalloy, *Mater. Sci. Eng. A*, 2004, **387–389**, p 728–733
13. E. Balikci, R.A. Mirshams, and A. Raman, Tensile Strengthening in the Nickel-Base Superalloy IN738LC, *J. Mater. Eng. Perform.*, 2000, **9**, p 324–329
14. I. Calliari, M. Magrini, and M. Dabalà, Microstructural Evolution of Udimet 720 Superalloy, *J. Mater. Eng. Perform.*, 1999, **8**, p 111–115
15. M. Lifshitz and V.V. Slyozov, The Kinetics of Precipitation from Supersaturated Solid Solution, *J. Phys. Chem. Solids*, 1961, **19**, p 35–50
16. C. Wagner, Theorie der Alterung von Niederschlagen Durch Umlosen, *Z. Electrochem.*, 1961, **65**, p 581–591 (in German)